



# Laboratory investigation into the use of soundless chemical demolitions agents for the breakage of hard rock

Kelly-Meriam Habib<sup>1</sup> · Isaac Vennes<sup>1</sup> · Hani Mitri<sup>1</sup>

Received: 14 March 2022 / Accepted: 26 August 2022  
© The Author(s) 2022

## Abstract

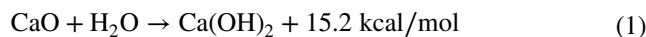
The method of drilling and blasting with explosives is widely used in rock fragmentation applications in the mining industry for mine development and ore production. However, the use of explosives is associated with rigorous safety and environmental constraints as blasting creates toxic fumes, ground vibrations, and dust. This study is focused on the use of Soundless Chemical Demolition Agents (SCDA) as a more environmentally friendly method for rock breakage and a potential replacement of explosives. In this paper, the results of a series of experimental tests are reported to identify the effect of SCDA on hard rock breakage under no load and under uniaxial loading conditions. Stanstead granite prismatic specimens of 152.4 mm (6") × 152.4–203.2 mm (6–8") × 406.4 mm (16") are used to test the influence of borehole size on the time to fracturing with SCDA borehole size of 25.4 mm (1"), 31.75 mm (1.25") and 38.1 mm (1.5"). It is shown that the fracturing time decreases with increasing borehole size. It is also shown that specimens subjected to uniaxial compression of 5 MPa fracture as early as 7 h after SCDA mixing. A borehole spacing to borehole diameter ratio of 12.8 to 14.6 is suggested for practical applications.

**Keywords** Explosive-free · Hard rock fragmentation · Soundless chemical demolition agents · Uniaxial loading

## 1 Introduction

The most conventional method of hard rock fragmentation in the mining industry is the drill and blast method. Commonly used explosives in the mining industry are ammonium nitrate fuel oil (ANFO), black powder, and to a lesser extent dynamite. Ammonium nitrate is an oxidizing agent that not only supplies oxygen to initiate and support combustion of the fuel, but it is also an explosive where on occasion ammonium nitrate can self-detonate posing a higher risk to workers (Farnfield and Wetherelt 2004). Given the risks posed by using explosives underground, along with the negative impacts such as the generation of toxic fumes and dust, there is a demand for alternative methods to fracture rocks. During the past three decades, several methods that have been proposed for rock fragmentation without explosives. Such methods include Thermal Fragmentation, Plasma Blasting, Controlled Foam Injection, Radial-Axial Splitter, and Supercritical Carbon Dioxide. More details on the pros and

cons of such methods are in (Habib et al. 2022). Soundless Chemical Demolition Agents (SCDA) is a promising method for rock fragmentation without explosives. SCDA, otherwise known as expansive cement, is a self-stressing cement containing Ordinary Portland Cement (OPC) and an expansive agent which is the source of the expansion pressure. The high expansion and hardening of the SCDA causes the breakage of the surrounding material such as rock (Taylor 1997). A common expanding agent is calcium oxide (CaO) where upon hydration, the generated calcium hydroxide crystals exert significant pressure in a confined space (Refer to Eq. (1)).



This explosive-free method has been explored by many researchers to optimize crack propagation in rock. Studies conducted by Hanif (2010) have investigated the effect of borehole spacing in granite rock to optimize crack propagation. It was shown that holes with gradually increasing spacing between consecutive holes cause the fracture to be initiated much sooner compared to the holes with uniform spacing (Hanif 2010). Gambatese (2003) studied controlled fracturing on concrete by introducing non-injected holes, and observed that cracks migrated to the non-injected holes

✉ Kelly-Meriam Habib  
kelly-meriam.habib@mail.mcgill.ca

<sup>1</sup> Department of Mining and Material Engineering, McGill University, Montreal, Canada

of the block (Gambatese 2003). Large scale studies done by Laefer et al. (2010) have tested breakage of concrete with the use of Bristar, a commercially available SCDA, testing several concrete blocks ( $0.76 \text{ m}^3$ ) of varying target strengths between 3.0 and 42.9 MPa with a central hole with 38 mm in diameter and 640 mm in depth. Key findings are that higher material strength took longer to initiate cracking and to obtain a 25.4 mm crack width. However, in a material having a tensile strength of less than 12 MPa, a cracking width of 25.4 mm was consistently observed within 24 h (Laefer et al. 2010). Small-scale laboratory experiments were conducted to test the efficacy of a commercially available SCDA, Betonamit, on norite rock subjected to uniaxial compression. Under uniaxial loading conditions, rock breakage occurs in the direction of the major principal stress. Under no load, rock breakage occurs in a randomized pattern. (Musunuri and Mitri 2009). Other works conducted by Habib (2019) have also investigated the effect of the addition of calcium chloride in SCDA to accelerate the breakage of crack initiation in concrete. It was shown that the addition of 3% of calcium chloride BWOW (by weight of water), that a higher degree of crack growth is noticed compared to the control sample without additive (Habib 2019). Gomez and Mura (1984) proposed a minimum spacing between SCDA holes to be less than 8 times the hole diameter for hard rocks, 8 to 12 times for medium hard rock, and 12 to 18 times the SCDA hole diameter for soft rocks (Gomez and Mura 1984). Arshadnejad et al. (2011) developed a more comprehensive empirical formula to estimate the optimal spacing in rock between holes in terms of hole diameter, expansive pressure as well as the material's tensile strength and fracture toughness (Arshadnejad et al. 2011). Apart from the extensive work done on breaking concrete and hard rock with the use of SCDA, much research has been dedicated to quantifying the pressure of SCDA using steel pipes. The most common experiment uses the thick-walled cylinder configuration where SCDA is poured into the cylinder or borehole and a strain gauge is affixed to the outer surface to record the tangential strain due to expansive pressure. This serves as the main output to estimate the pressure of SCDA (Soeda and Harada 1993; Hinze and Brown 1994; Hanif 2010; Laefer et al. 2010; Arshadnejad et al. 2011; Gholinejad and Arshadnejad 2012). The expansive pressure is estimated from the analytical equation of thick-walled cylinder subjected to internal pressure (Timoshenko and Goodier 1951). However, numerous studies neglected to consider the influence of the rigidity of the steel cylinder and its relation to that of rock. Since the effect of host rigidity is not well studied, the reported pressures may not be valid for rock. Moreover, given that the high heat of hydration associated with the chemical reaction of lime-based expansive cement (refer to Eq. (1)), can also affect the SCDA pressure, and since steel is highly conductive compared to rock, it is of critical

importance to estimate the pressure in real conditions such as in rock where a much higher heat sink is present.

So far it is known that the breakage of rock occurs when the tensile strength of the rock to be demolished is exceeded (Harada et al. 1989). However, it is not clear what the pressure evolution is over time up until crack initiation in rock. This study performs a series of experiments on granite slabs with a single SCDA hole under load and no load to retrieve raw strain measurements up until fracture for future work and to be used as a basis of calibration.

## 2 Experimental program

To begin, the influence of borehole diameter on SCDA in Stanstead granite slabs is investigated. The slab dimensions are  $152.4 \text{ mm}$  (6")  $\times$   $152.4\text{--}203.2 \text{ mm}$  (6–8")  $\times$   $406.4 \text{ mm}$  (16") and no load is applied. The tested borehole size diameters are  $25.4 \text{ mm}$  (1"),  $31.75 \text{ mm}$  (1.25") and  $38.1 \text{ mm}$  (1.5"). The second part of the experimental program studies the effect of SCDA-filled borehole subjected to uniaxial compressive stress with two borehole diameter sizes namely  $38.1 \text{ mm}$  (1.5") and  $44.45 \text{ mm}$  (1.75"). Commercially available SCDA selected for this study is Betonamit. All SCDA grouts are mixed consistently for 10 min and poured directly into the borehole. SCDA performance was assessed in three ways:

- (1) Measured strains around the borehole; 2 strain gauges, one above (SG1) and one below (SG3) the borehole, placed horizontally, and 2 strain gauges, one to the right (SG2) and one to the left (SG4) of the borehole, placed vertically (refer to Fig. 1 for the location of strain gauges).
- (2) Visual cracking with a time-lapse camera.
- (3) Time of first crack (TFC) and at time at which the slab is fully fractured.

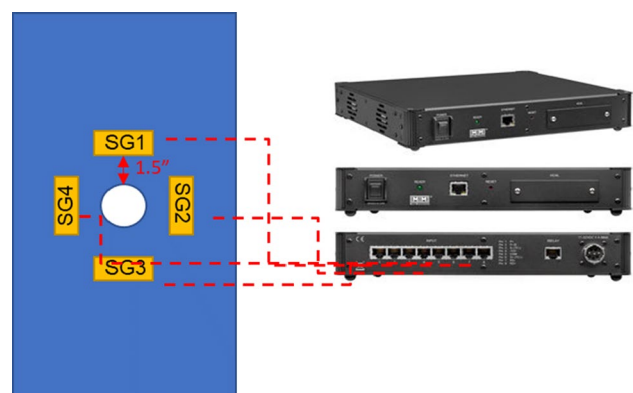


Fig. 1 Location of strain gauges

A total of 10 rock slabs were tested in this study. To identify each sample, the following nomenclature M-SL#-ID-HD-HL-L-XX was adopted.

- (1) M: Material, e.g., G for Granite.
- (2) SL#: Slab #, e.g., SL1 (152.4 mm (6") × 152.4 mm (6") × 406.4 mm (16")) or SL2 (152.4 mm (6") × 203.3 mm (8") × 406.4 mm (16"))
- (3) ID: Internal Diameter in inches, e.g., 125 for 158.75 mm (1.25") borehole.
- (4) HD: Hole Depth in inches, e.g., 625 for 158.75 mm (6.25")
- (5) HL: Hole location, e.g., M for middle, LT for lower third, UT for upper third
- (6) L: Loaded Slab at 5 MPa.
- (7) XX: Serial Number.

The hole depth was fixed at 4–5 times the SCDA hole diameter. The strain gauges were placed 38.1 mm (1.5") away from the edge of the borehole; 2 below and 2 on the sides (refer to Fig. 1). As shown in Fig. 2a), a 200-tonne uniaxial compression frame was used for the loaded specimens. For the loaded specimens, the top surface of the granite slab was greased with MoS<sub>2</sub> to reduce friction between the metal loading plate and the rock. Table 1 reports the configuration of the slabs tested in this study.

### 3 Results and discussion

#### 3.1 Rock characterization

A series of Brazilians tests were conducted to determine the tensile strength on the slabs (refer to Fig. 3 for test set-up). The Stanstead granite samples were cored from the granite slab and prepared in compliance with the ASTM D3967 Standard. The results give a mean value of 7.5 MPa with a standard deviation of 0.33.

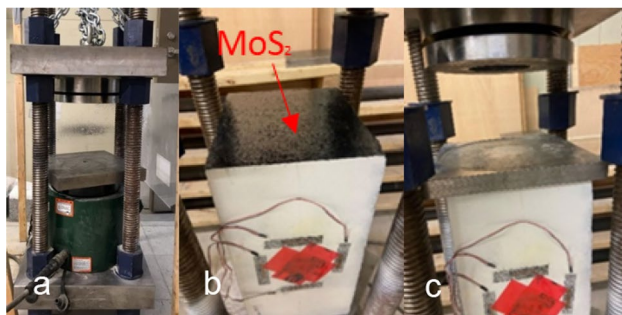


**Fig. 2** Test set-up for loaded specimens: **a** 200-tonne uniaxial compressive rig; **b** Greased top surface of rock specimen; **c** Metal loading plate placed on rock specimen

**Table 1** Description of tested specimens

Sample configuration	SCDA Borehole diameter	Borehole depth
G-SL1-100-500-M-01	25.4 mm (1.00")	127 mm (5.00")
G-SL1-100-500-M-02	25.4 mm (1.00")	127 mm (5.00")
G-SL1-100-500-M-03	25.4 mm (1.00")	127 mm (5.00")
G-SL2-125-625-M-01	31.75 mm (1.25")	158.75 mm (6.25")
G-SL2-125-625-M-02	31.75 mm (1.25")	158.75 mm (6.25")
G-SL2-150-600-M-01	38.1 mm (1.50")	152.4 mm (6.00")
G-SL2-150-600-M-02	38.1 mm (1.50")	152.4 mm (6.00")
G-SL2-150-600-UT-L	38.1 mm (1.50")	152.4 mm (6.00")
G-SL2-175-700-LT-L	44.45 mm (1.75")	177.8 mm (7.00")
G-SL2-175-700-M-L	44.45 mm (1.75")	177.8 mm (7.00")

#### 3.2 The influence of borehole size on granite

The effect of three borehole sizes (25.4 mm (1"), 31.75 mm (1.25") and 38.1 mm (1.5")) was investigated in a Stanstead granite slab with dimensions 152.4 mm (6") × 152.4 mm (6") × 203.2 mm (8") × 406.4 mm (16") (width × length × height). Each configuration was tested in duplicates to ensure repeatability and reliability. As shown in Fig. 1, the strain gauges were placed 38.1 mm (1.5") away from the borehole on each side, above and below borehole, and on the sides. The strains were measured until the first fracture appears, after which the strain gauges are potentially damaged due to localised splitting of the rock. The goal of the experiment is to identify the time of cracking using the measured strains in conjunction with timelapse photos of the slab.

Within a confined hole, radial pressure develops over time causing radial and tangential tensile stresses in the surrounding rock. A fracture is created at the weakest section along the inside surface of hole (Harada et al. 1989). The time



**Fig. 3** Brazilian test set-up on a Stanstead granite core

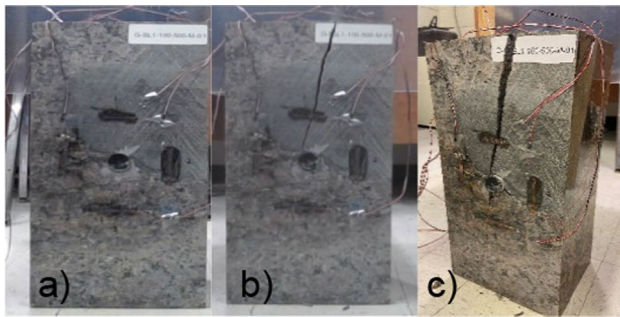


**Fig. 4** Slab G-SL1-100-500-M-01 **a** At time  $t_0$  **b** Initial breakage at time  $t_{18}$  **c** Complete breakage at time  $t_{24}$

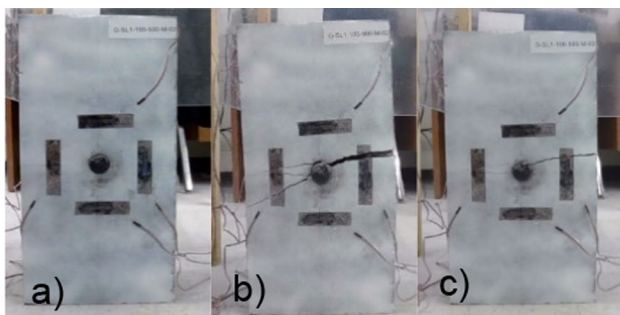


**Fig. 5** G-SL1-100-500-M-02 **a** At time  $t_0$  **b** Initial breakage at  $t_{15}$  **c** Complete breakage at  $t_{21}$

of cracking was identified by plotting the measured strains over time.

When the rock is undamaged, its reaction to the SCDA pressure is linear. Therefore, if the expansive pressure exerted by the SCDA is also linear, the measured strains will also increase linearly. Consequently, the strain at which this linear increase terminates, or the onset of nonlinear behaviour, is interpreted as an indication that cracking has initiated. This point is referred to in this work as the “critical strain”. On the other hand, both the time of visual fracture initiation and visual fracture completion were recorded, where the time of crack completion represents the point in time at which the fracture reaches the free surface of the slab. The 25.4 mm (1”) borehole is used as a base case to assess the time of fracturing with increasing borehole sizes (31.75 mm (1.25”) and 38.1 mm (1.5”). As shown in Figs. 4, 5, 6, for a 1” hole, the first fracture occurs at 18 h, 15 h, and 23 h for slabs M01, M02, and M03, respectively. Figures 7, 8 show the recorded strains for specimens G-SL1-100-500-M-02 and G-SL1-100-500-M-03. The strains for test G-SL1-100-500-M-01 were discarded. As summarized in Table 2, crack completion occurs after 21 to 27 h. As can be seen in Figs. 4, 5, 6, it takes on average 5 h after crack initiation for a crack to propagate to the free surface of the granite slab. As shown in Figs. 7, 8, the critical strain

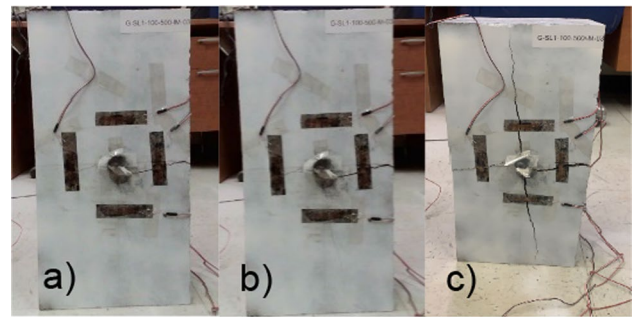


**Fig. 6** G-SL1-100-500-M-03 **a** At time  $t_0$  **b** Initial breakage at  $t_{23}$  **c** Complete breakage at  $t_{27}$

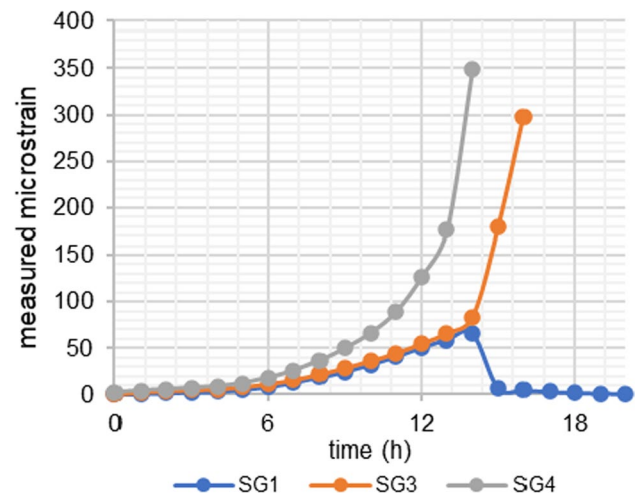


**Fig. 7** Measured strains in specimen G-SL1-100-500-M-02

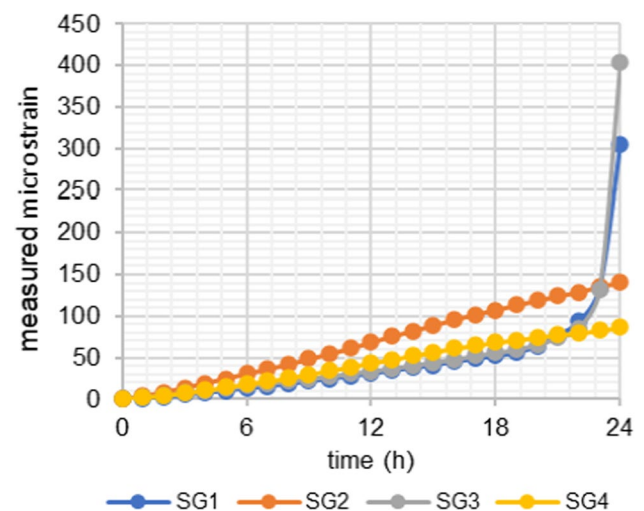


**Fig. 8** Measured strains in specimen G-SL1-100-500-M-03

**Table 2** Summary of test results under no load

Sample configuration	TFC (h)	Time of crack completion (h)
G-SL1-100-500-M-01	18	24
G-SL1-100-500-M-02	15	21
G-SL1-100-500-M-03	23	27
G-SL2-125-625-M-01	11.5	17
G-SL2-125-625-M-02	16	20
G-SL2-150-600-M-01	7.5	10
G-SL2-150-600-M-02	11	14

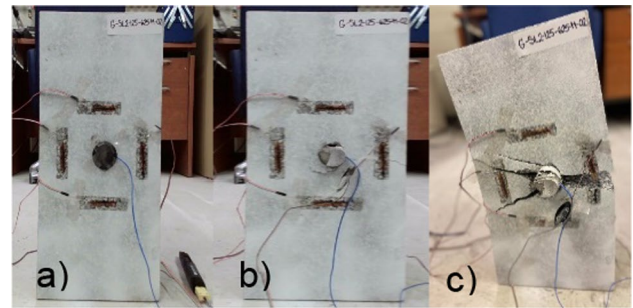


**Fig. 10** G-SL2-125-625-M-02 a At time  $t_0$  b Initial breakage at  $t_{16}$  c Complete breakage at  $t_{20}$

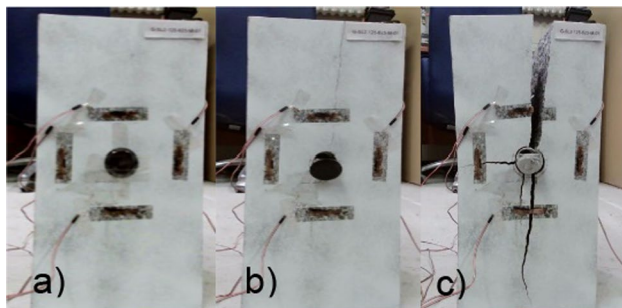


**Fig. 9** G-SL2-125-625-M-01 a At time  $t_0$  b Initial breakage at  $t_{11.5}$  c Complete breakage at  $t_{17}$

at which the linear behaviour ends for specimen G-SL1-100-500-M-02 and G-SL1-100-500-M-03 is 6 h and 19 h respectively. It is also apparent that the non-linear behaviour is exponential, suggesting that there has been significant brittle damage to the rock at those points. This is in accordance with the visual cracking at which the time of initial cracking for G-SL1-100-500-M-02 and G-SL1-100-500-M-03 occur at 15 h and 23 h respectively, both times at which the strains increase exponentially as shown in Figs. 7, 8 (SG2 was damaged at the beginning of the test and is therefore omitted from the results in Fig. 7). It is also shown that non-linear strain increase starts before cracking is visible on the slab surface, suggesting that visual identification of superficial cracking alone is not sufficient to determine the time at which fracturing initiates. This could be due to fracture initiating deeper in the block, or that the crack width is too small to capture with the camera.

The delay between visible crack initiation and non-linear strain increase is also observed in all specimens with an increased borehole size of 31.75 mm (1.25"). Specimens G-SL2-125-625-M-01 and G-SL2-125-625-M-02 show a TFC of 11.5 h and 16 h, respectively after SCDA is injected into the hole (refer to Figs. 9, 10 for visual cracking). The onset of non-linear behaviour for specimens G-SL2-125-625-M-01 and G-SL2-125-625-M-02 begins after 5 h and

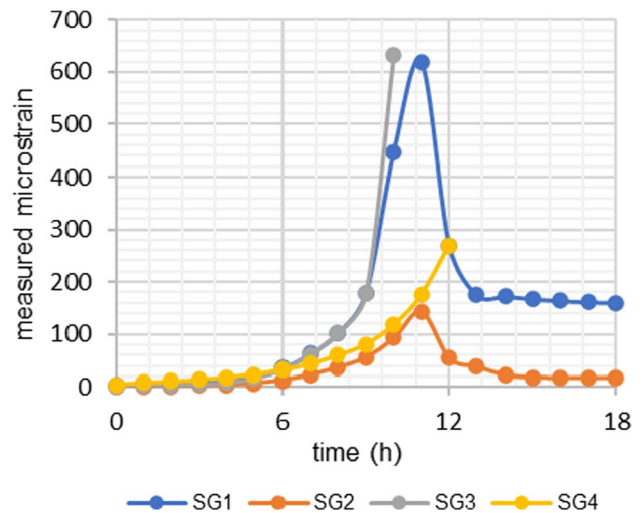


**Fig. 11** Measured strains in specimen G-SL2-125-625-M-01

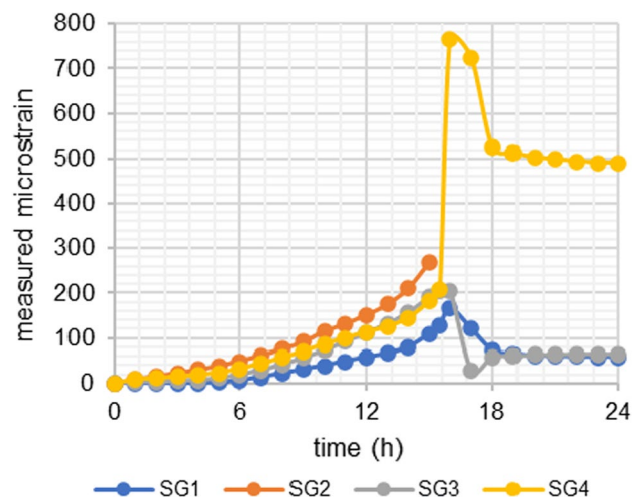


**Fig. 12** Measured strains in G-SL2-125-625-M-02

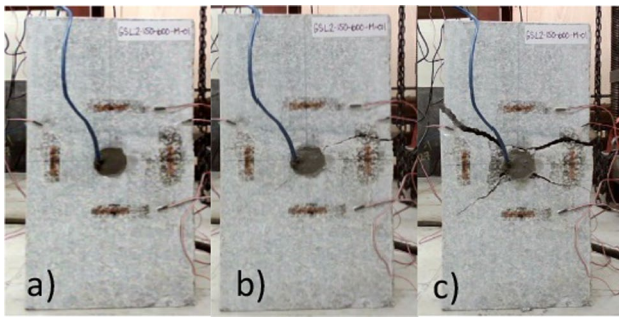


**Fig. 13** G-SL2-150-600-M-01 **a** At time  $t_0$  **b** Initial breakage  $t_{7.5}$  **c** Complete breakage  $t_{10}$

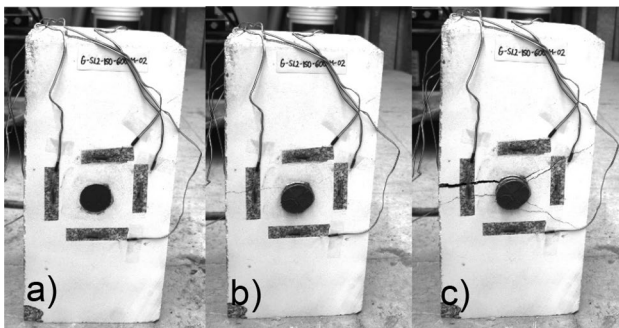


**Fig. 14** G-SL2-150-600-M-02 **a** At time  $t_0$  **b** Initial breakage  $t_{11}$  **c** Complete breakage at  $t_{13}$

8 h, respectively (refer to Figs. 11, 12 for strain values). The 31.75 mm specimens exhibited a faster reaction than the 25.4 mm where the time of initial cracking is decreased by an average of 5 h.

Compared to specimens, G-SL1-100-500-M-01, G-SL1-100-500-M-02, G-SL1-100-500-M-03, crack completion occurs slightly earlier between 17 and 20 h.

The sharp decrease in strains shown in Figs. 11, 12 is attributed to local stress relief due to cracking. When the strain gauges were not damaged, the observed relaxation corroborates with visual cracking.

With a 38.1 mm (1.5") SCDA injected hole, the time of breakage is reduced by half when compared to a 25.4 mm (1") hole. The TFC is also significantly decreased, at 7.5 h and 10 h for specimens G-SL2-150-600-M-01 and G-SL2-150-600-M-02 respectively. For both specimens, complete slab fracturing occurred relatively quickly after cracking initiated, in 2.5–4 h as shown in Figs. 13, 14, 15. Figure 15 shows the rapidly increasing strains after 7.5 h and quickly decreasing strains once the slab splits, indicating that the slab is fully relaxed, and all stresses have dissipated. Given that the strain gauges were not bisected by any cracks, the observed relaxation corroborates with the visual cracking. Figure 16 shows that at the time of visual breakage (11 h), a

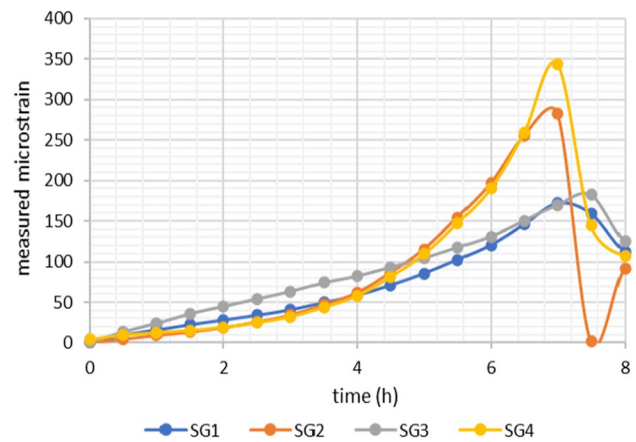


**Fig. 15** Measured strains of specimen G-SL2-150-600-M-01

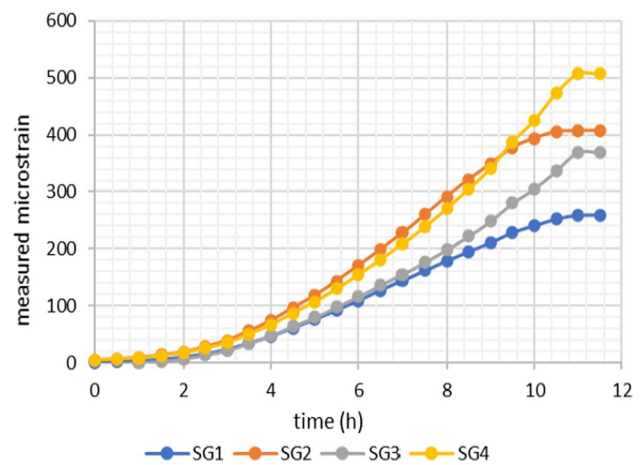


**Fig. 16** Measured strains in specimen G-SL2-150-600-M-02

small decay in strains is also observed shortly after indicating a relaxation of strains.

Overall, the specimens under no loading showed that visual cracking is delayed according to the measured strains. The measured strains indicate tensile damage in the slab before any superficial crack is apparent. This suggests that crack initiation may have occurred deeper in the slab before superficial cracking, or that the crack width is too small to observe. Therefore, the strain measurements are deemed a reliable tool to detect cracking without physical monitoring such as using a timelapse camera.

### 3.3 Effect of SCDA on rock breakage under load

The effect of uniaxial loading on rock breakage with SCDA was tested by subjecting a slab with a single SCDA-filled hole to uniaxial compressive stress using a 200-tonne uniaxial loading frame. This part of the study aims to quantify the fracture propagation rate of granite subjected to uniaxial

far-field pressure and radial pressure from the expansive cement. As shown in Table 1, a total of 3 specimens were tested under a uniaxial stress of 5 MPa. Such loading level was selected so that the tensile stresses around the hole do not exceed the tensile strength of the granite. All Stanstead granite slabs were 6" × 8" × 16", and three different hole locations were tested. All specimens were greased with a thin coat of MoS<sub>2</sub> to reduce friction between the rock and the loading plate as shown in Fig. 2b. As the first part of the investigation shows a decrease in TFC with the increase of borehole diameter, it was decided to adopt only the largest diameter of 38.1 mm (1.5") for the second part as uniaxial loading condition was thought to delay fracturing. To confirm the trend, another size of 44.45 mm (1.75") hole was also tested. Three specimens were tested; specimen G-SL2-150-600-UT-L with a 38.1 mm (1.5") SCDA hole located in the upper third of the slab, specimen G-SL2-175-700-M-L with a 44.45 mm (1.75") SCDA hole located in the middle of the slab and specimen G-SL2-175-700-LT-L with 44.45 mm (1.75") SCDA hole located in the lower third of the slab. Regarding the positioning of the holes, the goal is to observe the influence of hole diameter and its position on the TFC and time of complete breakage, all while monitoring the longest fracture path. Due to the limited number of samples available, it was not possible to return to the smaller SCDA hole sizes. The adopted holistic approach deemed adequate. As shown in Fig. 1, strain gauges were fixed 38.1 mm (1.5") away above (SG1) and below (SG3), and to the right (SG2) and left (SG4) side of the borehole. Both timelapse photos and strains were recorded to detect time of initial cracking and crack completion. Crack completion was assessed based on the time that cracking below and above the borehole reached the metal loading plates. As shown in Figs. 18, 20, 22, the strains for SG2 (right gauge) and SG4 (left gauge) remain in constant compression indicating that all slabs remained fully loaded over the entire duration of the test. As shown in Fig. 17b, a 38.1 mm (1.5") SCDA-filled hole located in the upper third of the slab (Specimen G-SL2-150-600-UT-L) shows initial cracking after 7 h and crack completion shortly after in 10 h. Figure 17b–d shows that initial cracking propagates towards upper metal loading plate end first and then to the lower plate 3 h later when complete breakage of the specimen has occurred.

As shown in Fig. 18, the measured strains for SG1 (strain gauge above the borehole) and SG3 (below the borehole) experience a sudden change in strain rate at 6 h leading to a TFC of 7 h.

This will help estimate an L/phi ratio to design the hole spacing in practical applications where uniaxial loading conditions are present. Figure 19b shows a 1.75" SCDA-filled hole located in the middle of the slab (G-SL2-175-700-M-L). Superficial cracking initiation is shown after 6.8 h and crack completion after 9.8 h. Compared to G-SL2-150-600-UT-L,

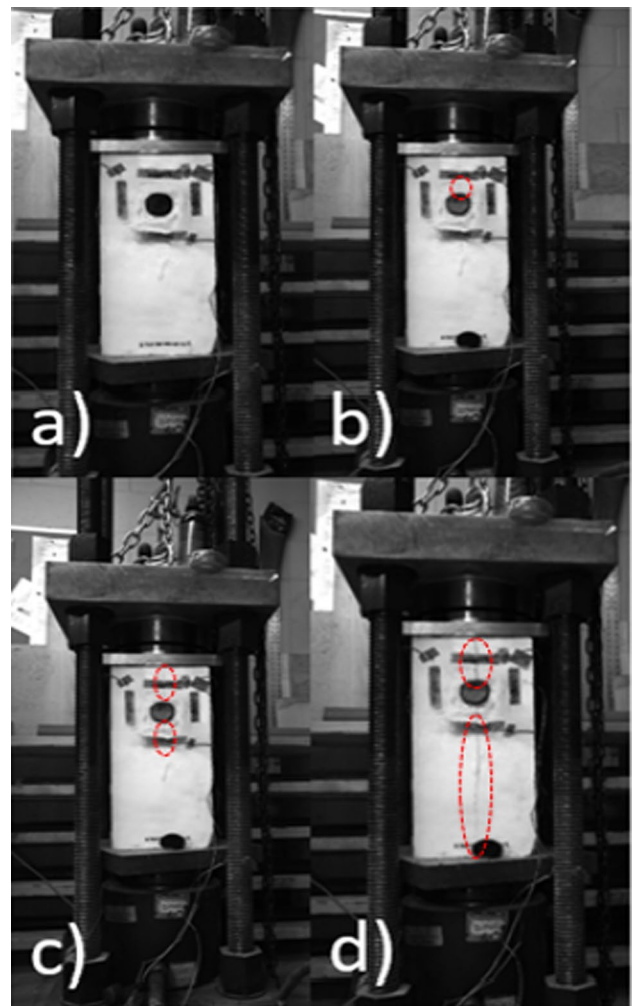


Fig. 17 G-SL2-150-600-UT-L a At time  $t_0$  b TFC at  $t_7$  c Breakage at  $t_{7.5}$  d Complete breakage at  $t_{10}$

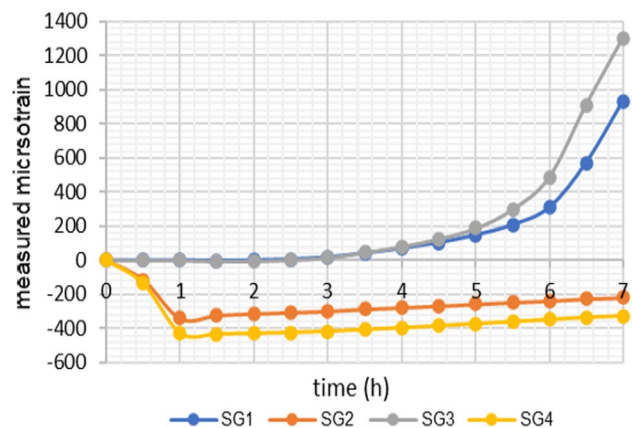
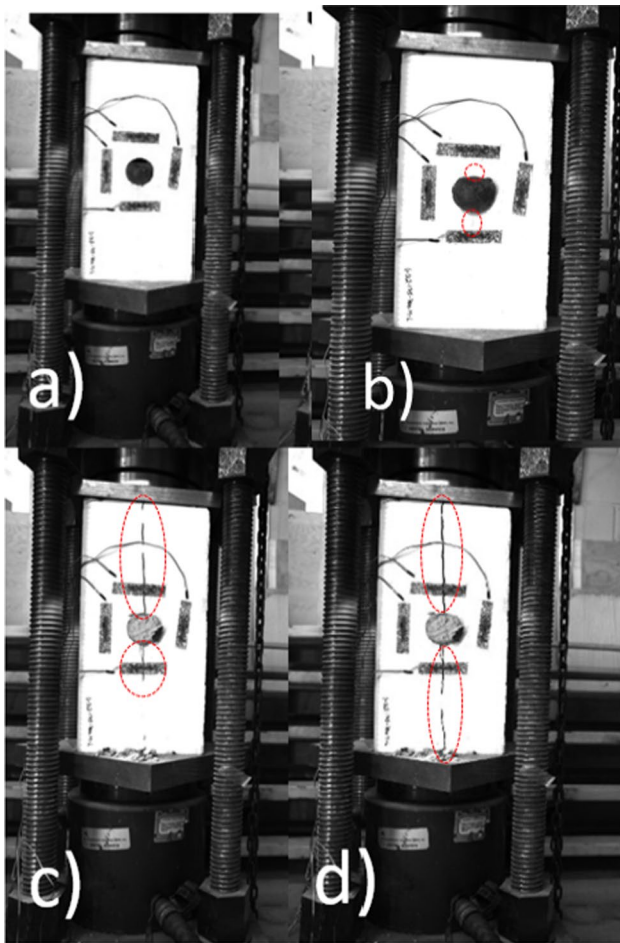
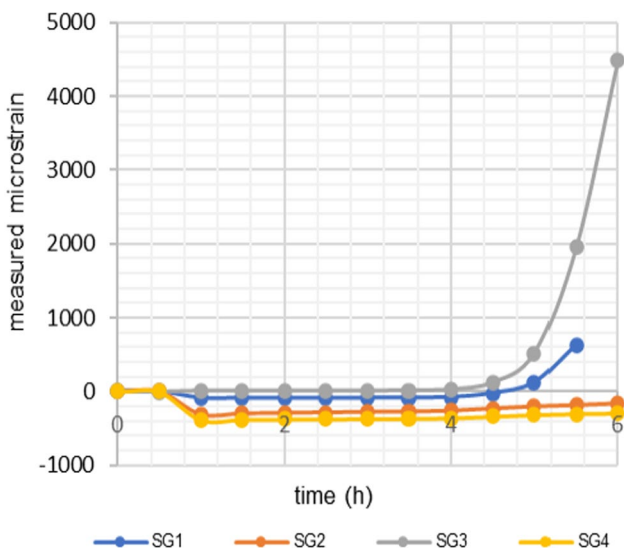


Fig. 18 Measured microstrain of specimen G-SL2-150-600-UT-L



**Fig. 19** G-SL2-175-700-M-L **a** At time  $t_0$  **b** Initial breakage  $t_{6.8}$  **c** Breakage at  $t_9$  **d** Complete breakage  $t_{9.73}$



**Fig. 20** Measured strains in specimen G-SL2-175-700-M-L

the time of initial fracture is very close and does not significantly differ from the time of complete fracturing. Similarly, the fractures above the borehole propagated to the greased upper plate before the crack below the borehole has reached the metal plate. As shown in Fig. 20, there is a sharp increase in the strain rate at 6 h before visual cracking is detected.

This shows that the visual behavior of cracking is once again delayed relative to the measured strains by 1 h. However, a different fracture pattern is observed with the 1.75" SCDA filled hole located in the lower third of the granite slab (G-SL2-175-700-M-L).

In this case, Fig. 21b shows initial cracking superficial cracking apparent after 7 h, in accordance with specimens G-SL2-150-600-UT-L and G-SL2-175-700-M-L. However, the crack fully propagated after 12 h, which is significantly longer than what was observed for the latter two specimens. Initial fracturing is also in accordance with the measured strains in Fig. 22 where an increase in strain is observed after 7 h. The fracture pattern differs from specimens from the two other specimens tested: G-SL2-150-600-UT-L and G-SL2-175-700-M-L.

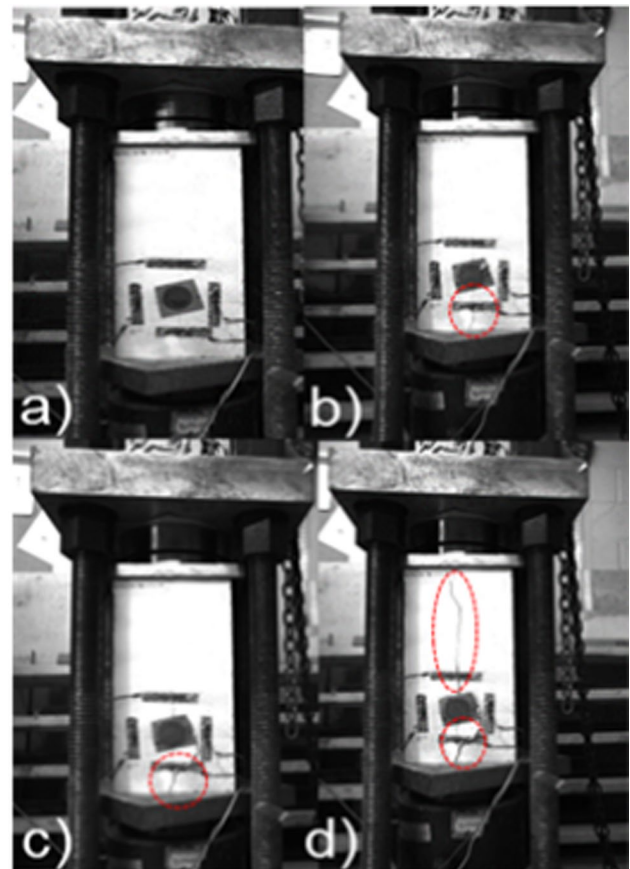


**Fig. 21** G-SL2-175-700-LT-L **a** At time  $t_0$  **b** Initial breakage **c** Breakage at  $t_7$  **d** Complete breakage at  $t_{12}$

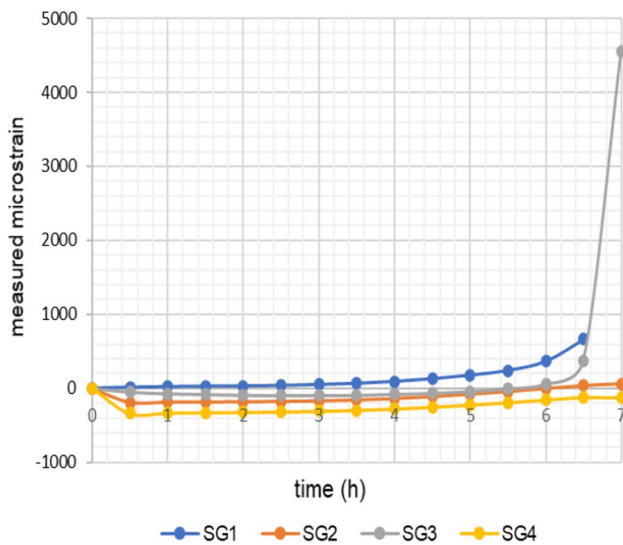


Fig. 22 Measured strains in specimen G-SL2-175-700-LT-L

As shown in Fig. 21c, cracking first propagates towards the lower metal plate and then propagates slowly towards the greased upper metal loading plate. The delay in fracture completion can therefore be related to the non-greased bottom plate offering increased frictional resistance, resisting the separation of the two slab halves.

As shown in Fig. 21c, cracking first propagates towards the lower bearing plate and then propagates slowly towards the greased upper loading plate. The delay in fracture completion can therefore be related to the non-greased bottom plate offering increased frictional resistance, resisting the extension strain that causes slab separation. Overall, Figs. 17, 19, 21 show that all fractures propagate in the direction of the major principal stress, unlike the unloaded

slabs where fracturing generally propagated towards some or all the nearest faces. Since the loaded specimens had directional cracking as opposed to the unloaded specimens, optimal borehole spacing can be estimated. The ratio of the length of fracture over the SCDA hole diameter ( $\Phi$ ) is an indicator for maximum hole spacing. As each SCDA can generate a fracture length  $L_f$ , the spacing,  $S$ , between two SCDA holes is calculated as  $S=2L_f/\Phi$ . As shown in Table 3, the illustration for each specimen depicts which end of the granite slab is used to measure the length of fracture. The length  $L_f$  was selected based on the longest crack path measured from the borehole center. As the specimens have different hole configurations, it should be noted the  $L_f/\Phi$  ratio reported in Table 3 is not a direct comparison between the specimens to judge their performance. Rather, it is used to help delineate the required SCDA borehole spacing in practice. As can be seen in Table 3, the  $L_f/\Phi$  ratio for the loaded granite can be up to 6.4 to 7.3. As the top surface is greased, it acts as a line of symmetry. Thus, for practical applications, it can be claimed that the maximum allowable spacing between two SCDA boreholes is  $2L_f/\Phi$ , or 12.8 to 14.6 $\Phi$  to achieve complete fracturing. According to work done by Gomez and Mura (1984), a proposed spacing between SCDA holes of  $8\Phi$  is suggested (Gomez and Mura 1984), however, for unloaded specimens.

### 4 Conclusions

In this paper, the results of a series of experimental tests are reported to identify the effect of SCDA on hard rock breakage under no load and under uniaxial loading conditions. Stanstead granite specimens of 152.4 mm (6")  $\times$  152.4 mm–203.2 mm (6–8")  $\times$  406.4 mm (16") are

Table 3 Summary of  $L_f/\Phi$

Specimen ID	G-SL2-150-600-UT-L	G-SL2-175-700-M-L	G-SL2-175-700-LT-L
Specimen configuration			
SCDA hole size	31.8 mm (1.5")	44.45 mm (1.75")	44.45 mm (1.75")
TFC (h)	7	6.8	7
Complete breakage (h)	10	9.7	12
$L_f/\Phi$	7.3	4.6	6.4

used to test the influence of borehole size on the fracturing time with 25.4 mm (1"), 31.75 mm (1.25") and 38.1 mm (1.5") SCDA holes under no load. It is shown that fracturing time decreases with increasing borehole size. The time of initial fracturing for a 38.1 mm (1.5") borehole size is half of that of a 1" filled SCDA hole. Moreover, the measured strains for all specimens increase exponentially at some point in time, and this exponential behavior is interpreted as tensile damage progression in the slab. The results demonstrate that strain measurement is a reliable indicator for fracture initiation, and that this fracture initiation could not be detected visually. Another series of tests were performed to verify the influence of a uniaxial pressure of 5 MPa on the slab fracturing with SCDA. Three tests with a single SCDA hole at 3 different locations were tested: 38.1 mm (1.5") borehole size in the upper third of the slab (G-SL2-150-600-UT-L), 1.75" in the middle of the slab (G-SL2-175-700-M-L) and 1.75" in the lower third of the slab (G-SL2-175-700-LT-L). SCDA expansion-initiated fracturing as early as 7 h for all tests. Specimens SL2-150-600-UT-L and G-SL2-175-700-M-L split after 10 h, whereas specimen G-SL2-175-LT-L split after 12 h. The delay in fracturing completion could be due to the non-greased bottom plate resisting fracture propagation due to the increased friction. Based on the experimental results, the fracture length to borehole diameter ratio  $L/\Phi$ , was calculated to estimate the maximum allowable spacing between SCDA holes subjected to uniaxial stress. It is suggested that the spacing between SCDA boreholes be  $12.8\text{--}14.6\Phi$  for practical applications involving uniaxial compression. Such higher borehole spacing suggestion for loaded samples than the  $8\Phi$  for unloaded sample suggested by Gomez and Mura (1994) implies that uniaxial loading is beneficial for hard breakage with SCDA.

**Acknowledgements** This work was financially supported by a research grant from Natural Resources Canada, Clean Growth Program, Grant No. CGP-17-1003 and industry partner Newmont Corporation. The authors are grateful for their support.

**Author contributions** KH: conceptualization, methodology, experiments, analysis, and production of the first draft, IV: technical insight, support for experiments, and first review, HM: supervision, revision, and funding acquisition. All authors read and approved the final manuscript.

**Open Access** This article is licensed under a Creative Commons Attribution 4.0 International License, which permits use, sharing, adaptation, distribution and reproduction in any medium or format, as long as you give appropriate credit to the original author(s) and the source, provide a link to the Creative Commons licence, and indicate if changes

were made. The images or other third party material in this article are included in the article's Creative Commons licence, unless indicated otherwise in a credit line to the material. If material is not included in the article's Creative Commons licence and your intended use is not permitted by statutory regulation or exceeds the permitted use, you will need to obtain permission directly from the copyright holder. To view a copy of this licence, visit <http://creativecommons.org/licenses/by/4.0/>.

## References

- Arshadnejad S, Goshtasbi K, Aghazadeh J (2011) A model to determine hole spacing in the rock fracture process by non-explosive expansion material. *Int J Miner Metall Mater* 18:509–514. <https://doi.org/10.1007/s12613-011-0470-5>
- Farnfield R, Wetherelt A (2004) After-blast fumes from ANFO mixtures. *Quarry Manag* 31(2):11–19
- Gambatese JA (2003) Controlled concrete demolition using expansive cracking agents. *J Constr Eng Manag* 129:98–104
- Gholinejad M, Arshadnejad S (2012) An experimental approach to determine the hole-pressure under expansion load. *J South African Inst Min Metall* 112:631–635
- Gómez C, Mura T (1984) Stresses caused by expansive cement in borehole. *J Eng Mech* 110(6):1001–1005
- Habib K (2019) Laboratory investigation into soundless chemical demolition agents for rock breakage in underground mines. M.Sc. thesis. McGill University, Montreal, QC
- Habib KM, Shnorhokian S, Mitri H (2022) Evaluating the application of rock breakage without explosives in underground construction—a critical review of chemical demolition agents. *Minerals* 12(2):220
- Hanif M (2010) Effective use of expansive cement for the deformation and fracturing of granite. *Gazi Univ J Sci* 20:1–5
- Harada T, Idemitsu T, Watanabe A, Takayama S (1989) The design method for the demolition of concrete with expansive demolition agents. In: Shah SP, Swartz SE (eds) *Fracture of concrete and rock*. Springer, New York, pp 47–57
- Hinze J, Brown J (1994) Properties of soundless chemical demolition agents. *Constr Eng Manag* 120:816–827. [https://doi.org/10.1016/0148-9062\(95\)93364-U](https://doi.org/10.1016/0148-9062(95)93364-U)
- Laefer DF, Ambrozevitch-Cooper N, Huynh MP (2010) Expansive fracture agent behaviour for concrete cracking. *Mag Concr Res* 62:443–452. <https://doi.org/10.1680/macr.2010.62.6.443>
- Musunuri A, Mitri H (2009) Laboratory investigation into rock fracturing with expansive cement. *Int J Min Miner Eng* 1:327–345. <https://doi.org/10.1504/IJMME.2009.029318>
- Soeda K, Harada T (1993) The mechanics of expansive pressure generation with expansive demolition agent. *Trans. Jpn Soc Civ Eng* 19:121–135
- Taylor HF (1997) *Cement chemistry*. Thomas Telford, London
- Timoshenko S, Goodier J (1951) *Theory of elasticity*. *Phys Contin Media* 6:234–259

**Publisher's Note** Springer Nature remains neutral with regard to jurisdictional claims in published maps and institutional affiliations.